Optics Communications 281 (2008) 5973–5981

Contents lists available at ScienceDirect

Optics Communications

journal homepage: www.elsevier.com/locate/optcom

Analysis of electrically configurable spectral phase encoding techniques for optical CDMA

A. Andueza *, D. Lasaosa, D. Benito

Department of Electrical and Electronic Engineering, Public University of Navarra, Campus de Arrosadia s/n, 31006 Pamplona, Spain

ARTICLE INFO

Article history:
Received 23 May 2008
Received in revised form 27 August 2008
Accepted 27 August 2008

ABSTRACT

We present the theoretical analysis and simulation of an encoder/decoder pair with applications in Optical Code Division Multiple Access (OCDMA) systems. The theory and simulations presented are valid for any technique that relies on the combination of dispersion/phase modulation/dispersion for spectral phase encoding. We perform a theoretical study of the system, characterizing its main limiting factors, and a comparative study of the Multi-Access Interference (MAI) and Bit Error Rate (BER) for a simple multi-user system at high-bit rate in a Passive Optical Network (PON) environment. The capacity of the system to carry out error-free operation for codes of different length and with different numbers of users is also demonstrated through simulation.

1. Introduction

Due to the exponential growth telecommunications optical access networks are currently undergoing, various techniques have been studied and developed for use in Optical Code Division Multiple Access (OCDMA) networks as alternatives to the traditional optical multiplex access methods based on Time Division Multiplex (TDM) and Wavelength Division Multiplex (WDM). OCDMA is a new optical multiplexing technique that is attracting great interest for its potential applications in the broadband multi-access network environment, especially in local area networks and Passive Optical Networks (PON) [1–3]. Asynchronous network access, high bit rate for the user, improved security, simplified network management, higher optical bandwidth for each user and scalability are some of its outstanding features.

Time-domain one-dimensional Direct Sequence OCDMA (DS-OCDMA) has been proposed for coherent and incoherent systems with Superstructured Fiber Bragg Gratings (SSFBGs) [4–6], optical delay lines [7] and Long-Period Fiber Grating (LPGs) [8]. Two-dimensional OCDMA technique is named indistinctly Fast Frequency Hopping (FFH-OCDMA) or Wavelength-Hopping Time-Spreading (WH-TS-OCDMA), and differs from other OCDMA techniques since it uses coding simultaneously in time and frequency domains. Following this scheme, multiple coherent and incoherent FFH-OCDMA systems have been reported. These systems are mainly based on optical grating devices such as Array Waveguide Gratings (AWGs) [9], Chirped Moiré Gratings (CMGs) [10], optical interferometers, optical time delay lines [11], Holographic Bragg Reflectors (HBRs) [12], lenses working with spatial gratings [13] and sampled FBGs [14]. Yet another OCDMA method is Frequency-Encoded OCDMA (FE-OCDMA), which does, in the frequency domain, an analogous process to that which DS-OCDMA coding does in the time domain. This technique has been implemented in both coherent and incoherent systems using passive optical devices such as Superimposed FBGs (SFBGs) [15], phase and amplitude mask combined with spatial gratings [16–18], Fiber Bragg Gratings [19,20] and Integrated Rings Resonators Circuits [21].

Especially interesting is the FE-OCDMA technique, which presents some advantages, including the ability to use different types of optical codes, broadband sources or short pulses, complementary transmission and balanced reception. Furthermore, this method may be implemented using low-cost, easily fabricated, low-loss components.

In this paper we present a full theoretical analysis, including system performance simulation, of an alternative approach for OCDMA encoder/decoder, based on a combination of Linearly Chirped Fiber Bragg Gratings (LCFBG) and phase modulator (PM). This system was, to the best of our knowledge, first outlined in [20], a practical detailed implementation was first proposed in [22], and proof of principle was recently achieved [23]. Making use of LCFBGs as dispersive media [24–26], and an electro-optical phase modulator (PM), a phase code is engraved on the frequency components of the data signal. The features of this proposed system make the encoder/decoder independent of the code family and length, since reconfiguration of the applied code is achieved simply by modifying the electrical signal that controls the PM. Furthermore, the encoder/decoder is more versatile because physical implementation does not depend on the code and the encoder/decoder used in the optical network can be the same for every user.

* Corresponding author. Tel.: +34 620 100 971; fax: +34 948 169 720.
E-mail addresses: angel.andueza@unavarra.es (A. Andueza), daniel.lasaosa@unavarra.es (D. Lasaosa), dbenito@unavarra.es (D. Benito).

0030-4018/$ - see front matter © 2008 Elsevier B.V. All rights reserved.
doi:10.1016/j.optcom.2008.08.050

Therefore, the encoder/decoder can be easily adapted if any network parameters are modified. Nevertheless, the encoder/decoder has the inconvenience of having a chip rate (for the electrical code applied in the PM) which is higher than the data bit rate used. However, this high-speed signal does not imply any limitation with currently available commercial components. In this paper, we perform a theoretical analysis, and evaluate through simulation the performance of the electrically-configurable FE-OCDMA encoder/decoder at standard transmission speed (0.622 Gbit/s) employing orthogonal codes of length 16 and 32 bits, for the cases of single and multiple users.

2. Theoretical analysis

In this section, we analyze the system performance in a single-user configuration, in order to obtain the main limiting factors and establish design rules and component characteristics. It is important to note that the theory presented is valid for any encoder/decoder that relies on dispersion for pulse broadening, producing the time separation of its original frequency components, followed by phase modulation for spectral phase encoding/decoding, and dispersion again to reconstruct a short pulse. The theoretical analysis presented uses a completely generic description for dispersive elements and phase modulation, or its results will be valid for general techniques [20], as well as for our proposed configuration [22], and even for a recently, experimentally demonstrated system [23]. Our proposed encoder encoder/decoder is composed by two LCFBGs, two optical circulators, and an electro-optic Phase Modulator (PM) [22], although alternative methods may be used for encoding and decoding [23]. In order to enhance the dispersion process at the LCFBG, the use of Gaussian optical pulses at data speed R_b with a linear prechirp are proposed, each pulse being described by

$$s_1(t) = \mathrm{Re}\{S_{1,l}(t)\cdot \exp(\mathrm{j}2\pi f_c t)\}, \tag{1a}$$

$$s_{1,l}(t) = A_0 \cdot \exp\left(-\frac{1+\mathrm{j}C}{2}\left(\frac{t}{T_0}\right)^2\right), \tag{1b}$$

where $S_{1,l}(t)$ is the low-frequency complex envelope, f_c is the optical carrier frequency, A_0 is the (in general complex) peak amplitude, C is the linewidth enhancement factor or prechirp, and T_0 is a measure of the pulse time width. Actually, $T_{FWHM} = 2(\ln 2)^{1/2}T_0 \approx 1.665T_0$, where T_{FWHM} is the Full-Width Half-Maximum (FWHM) time duration. The Fourier transform of the complex envelope is given by

$$S_{1,l}(f) = A_0 T_0 \sqrt{\frac{2\pi}{1+\mathrm{j}C}}\cdot \exp\left(-\frac{2\pi^2 T_0^2 f^2}{1+\mathrm{j}C}\right). \tag{2}$$

Hence, the FWHM bandwidth of the optical pulse source B_1 is given by

$$B_1 = \frac{\sqrt{(1+C^2)\ln 2}}{\pi T_0}. \tag{3}$$

In the following analysis, we will assume ideal LCFBGs, used as dispersion medium in order to impose a linear and fixed group delay in the data signal [27,28]. The transfer function of each dispersive device (assumed lossless) may be approximated by expressing its argument as a Taylor series:

$$H_i(f) \approx \cdot \exp(\mathrm{j}\Phi_i)\cdot \exp\left(\mathrm{j}2\pi\Phi_i'(f-f_c)\right)\cdot \exp\left(\mathrm{j}2\pi^2\Phi_i''(f-f_0)^2\right), \tag{4}$$

where Φ_i, Φ_i' Φ_i'' are the values of the argument and its two first derivatives with respect to angular frequency, respectively, evaluated at the central frequency of the optical pulse f_c; higher order terms have been neglected. Note that the first term in the Taylor expansion introduces a constant phase which will modify only the phase of the complex amplitude A_0, whereas the second term introduces a time delay constant for all frequencies. Thus, assuming a varying time-frame along the link such that the pulse center happens at $t = 0$ at any position, the effect of the third (quadratic) term is the only one to produce any effect on the pulse characteristics (note that loss, i.e., $|H_i(f)| < 1$, would also produce no significant effect on the pulse shape if it may be assumed to be close to constant in the operation bandwidth). Therefore, the spectrum of the complex envelope at the output of the first LCFBG is that of a linearly chirped Gaussian pulse [24,28],

$$S_{2,l}(f,\Phi_1'') = A_0 T_0 \sqrt{\frac{2\pi}{1+jC}}\cdot \exp\left(-2\pi^2 f^2\left(\frac{T_0^2}{1+jC} - j\frac{\Phi_1''}{2}\right)\right), \tag{5a}$$

where the dependence on Φ_1'' explicitly expresses the effect of the LCFBG dispersion on the pulse shape. The time-domain complex envelope is obtained through inverse Fourier transformation:

$$s_{2,l}(t,\Phi_1'') = A_0' \cdot \exp\left(-\frac{1+jC'}{2}\left(\frac{t}{sT_0}\right)^2\right), \tag{5b}$$

where A_0' and C' are the amplitude and linear chirp of the output pulse, respectively, and s is the time expansion factor. These dispersion-dependent parameters are written as

$$C' = C + \frac{(1+C^2)\Phi_1''}{2T_0^2}, \tag{6a}$$

$$s = \sqrt{\left(1+\frac{C\Phi_1''}{2T_0^2}\right)^2 + \left(\frac{\Phi_1''}{2T_0^2}\right)^2}, \tag{6b}$$

$$A_0' = \frac{A_0}{\sqrt{s}}\exp\left(j\frac{1}{2}\arctan\left(\frac{\Phi_1''}{2T_0^2 + C\Phi_1''}\right)\right). \tag{6c}$$

There is a compromise between the design parameters of the LCFBG and the Gaussian pulse source which determines the optimum pulse to be employed. It is well-known that the bandwidth-group delay product for a given LCFBG length is constant, therefore a narrow bandwidth will generate a high dispersion slope Φ_i'' and *vice versa*. The optical pulse prechirp allows a faster dispersion, relaxing the bandwidth demand an allowing a more realistic LCFBG design. Maximum time spreading of the pulses at the LCFBG output will be limited by the inverse of the data bit-rate. Therefore, the necessary prechirp value C may be determined by equating the output pulse time width to the inverse of the data bit-rate.

It follows from (5b) that the instantaneous frequency of the pulse at the LCFBG output is

$$f_i(t) = f_c - \frac{C'}{2\pi s^2 T_0^2}t. \tag{7}$$

The operation principle of the system is based on this relation between time and wavelength when the signal emerges from the LCFBG. The effect generated by the LCFBG is an ordering of the wavelengths present in each pulse, so that each wavelength is found at a different instant (see for example [24,25]). When the signal reflected from the LCFBG reaches the PM, an additional phase (t) is introduced for each wavelength in the pulse spectrum. This phase $\phi(t)$ is governed by the electrical code introduced in the PM electrodes; ideally, it is proportional to the electrical voltage $V(t)$. Consequently, it is easy to control the variation of the phase electrically, by modifying the signal code in order to assign different phase shifts for each wavelength. Furthermore, the coding technique is very flexible since both code length and code family may be modified without altering the system. For an applied phase shift $\phi_c(t)$, the pulse complex envelope at the output of the PM is given by

$$s_{3,l}(t,\Phi_1'') = A_0' \cdot \exp\left(-\frac{1+fC'}{2}\left(\frac{t}{sT_0}\right)^2\right) \cdot \exp(f\phi_c(t)). \quad (8)$$

The mathematical analysis of this complex envelope and the effect of its propagation throughout the rest of the system is significantly simplified by assuming a periodic phase shift $\phi_c(t)$. This is possible since, as most of the energy in a Gaussian pulse is contained within an interval of approximately three times its FWHM time duration, a periodic repetition of $\phi_c(t)$ outside this interval would have a negligible effect on the overall signal. We will discuss how this approximation simplifies the theoretical analysis. Under this assumption, the factor describing the phase-shift may be expressed as a Fourier series,

$$\exp(f\phi_c(t)) = \sum_{n=-\infty}^{+\infty} c_n \exp(f2\pi n f_p t), \quad (9)$$

where f_p is the repetition frequency assumed for $\phi_c(t)$. Note that as the repetition period $T_p = 1/f_p$ becomes larger compared to the pulse width sT_0, the approximation is closer to the exact result. However, very good approximations may be expected for $T_p > 4sT_0$. The spectrum of the modulated signal is therefore given by

$$S_{3,l}(f) = \sum_{n=-\infty}^{+\infty} c_n S_{2,l}(f - nf_p). \quad (10)$$

Since the instantaneous power in Eq. (9) is constant and equal to 1, it is trivial to find that the Fourier series coefficients c_n obey the relations

$$\sum_{n=-\infty}^{+\infty} c_n c_{n+m}^* = \delta_m, \quad (11)$$

where δ_m is Kronecker's delta symbol, having value 1 if $m = 0$, and value 0 otherwise.

The second LCFBG presents an opposite dispersion slope $\Phi_2'' = -\Phi_1''$, in order to compensate for the dispersive effect of the first one. Perfectly matched LCFBGs cannot be produced. However, tunable dispersion compensation may be achieved [24]. Furthermore, a certain dispersion mismatch is perfectly tolerable, as we will show later.

The effect of the second LCFBG in the encoder, the optical fiber used for transmission, and the first LCFBG in the decoder (ideally match to the first LCFBG in the encoder) may be lumped together and described through a net dispersion between modulators $\Delta\Phi''$. Thus, the spectrum of the complex envelope corresponding to the signal arriving into the PM in the decoder subsystem is

$$S_{4,l}(f) = \sum_{n=-\infty}^{+\infty} c_n S_{2,l}(f - nf_p, \Phi_1'') \exp\left(j2\pi^2 \Delta\Phi'' f^2\right). \quad (12)$$

Note that in the absence of phase modulation in the encoder (i.e., $c_n = \delta_n$), $S_{4,l}$ may be obtained from $S_{2,l}$ by substituting Φ_1'' by $\Phi_1'' + \Delta\Phi''$. In the presence of PM in the encoder,

$$S_{4,l}(f) = \sum_{n=-\infty}^{+\infty} c_n \exp\left(j\pi n^2 f_p \tau + j2\pi n(f - nf_p)\tau\right) \times S_{2,l}(f - nf_p, \Phi_1'' + \Delta\Phi''), \quad (13a)$$

$$S_{4,l}(t) = \sum_{n=-\infty}^{+\infty} c_n \exp\left(j\pi n^2 f_p \tau\right) \exp(j2\pi n f_p t) \times S_{2,l}(t + n\tau, \Phi_1'' + \Delta\Phi''), \quad (13b)$$

where we have defined

$$\tau = 2\pi\Delta\Phi'' f_p. \quad (14)$$

In other words, the signal arriving to the decoder PM is a series of linearly chirped, dispersion broadened Gaussian pulses with slightly different central frequencies, the pulses being ordered in time with equal separation between them from higher to lower central frequency or *vice versa*, depending on the sign of the net dispersion between modulators $\Delta\Phi''$.

The drive voltage applied to the decoder PM will be also assumed to be periodic, with the same repetition frequency f_p. We will write the phase shift introduced by the decoding PM as

$$\exp(-f\phi_d(t)) = \sum_{n=-\infty}^{+\infty} c_n'^* \exp(-f2\pi n f_p t), \quad (15)$$

where x^* denotes the complex conjugate of x. For matching encoder/decoder subsystems (i.e., for a desired user in an OCDMA system), $\phi_d(t)=\phi_c(t)$, or $c_n' = c_n$. After phase demodulation, we obtain

$$s_{5,l}(t) = \sum_{n=-\infty}^{+\infty} \exp\left(j\pi n^2 f_p \tau\right) c_n''(t) s_{2,l}(t + n\tau, \Phi_1'' + \Delta\Phi''), \quad (16)$$

where we have defined

$$c_n''(t) = \sum_{m=-\infty}^{+\infty} c_n c_m'^* \exp(j2\pi(n-m)f_p t). \quad (17)$$

Note that the output of the PM modulator is again the sum of identical dispersion-broadened pulses, each affected by a time delay, phase shift and weight function $c_n''(t)$. Note that the assumption of periodicity for the phase coding signal allows the expression of the received electrical signal as a sum of gaussian pulses with different amplitudes and phases. This would clearly simplify numerical calculations, as opposed to having the received electrical signal expressed as a convolution integral. However, this assumption has far more reaching consequences: note first that in the case of a non-periodic phase coding signal, the left-hand side in Eq. (10) would contain a convolution integral instead of a sum, highly increasing the difficulty of all subsequent derivations. Moreover, the expression of the output signal as in Eq. (16) allows a more intuitive explanation of the final results, as discussed in the rest of this paragraph.

For a desired user, as expected,

$$\sum_{n=-\infty}^{+\infty} c_n''(t) = \sum_{k=-\infty}^{+\infty} \exp\left(j2\pi k f_p t\right) \sum_{n=-\infty}^{+\infty} c_n c_{n-k}^* = 1 \quad (18)$$

However, since each weight function is in itself a Fourier series, the constant terms in all series add up to 1, while the non-constant terms (kth harmonic for nonzero k) cancel out. We therefore propose to approximate the weight functions $c_n''(t)$ by their average values. This approximation may be justified as follows: the sum of all coefficients for the kth harmonic, each one of them stemming from each one of the $c_n''(t)$, is zero. Therefore, we may view it as a large collection of complex numbers with zero sum (large because the optical bit rate is quite larger than the electrical bit rate). If we were to add a random phase to each one of this collection of vectors, the expectation value of their sum would still be zero. The variance of this sum, divided by the sum of the square of their moduli (which is in turn comparable to the average value of sum of the $c_n''(t)$), is approximatedly $1/N$, where N is the number of such vectors. Assuming that the optical bit rate is 16 times the electrical bit rate, about 50 coeficients will be relevant, yielding a variance for the kth harmonic in the sum of the $c_n''(t)$ in the order of 2% of its average value. Although the phase shift $\exp(j\pi n^2 f_p \tau)$ is not random, for large values of τ its behaviour is erratic enough to produce the same result, while for very small values of τ, its effect may be altogether neglected. The approximation may then be expected to produce good results, especially as the optical bit rate increases with respect to the electrical bit rate. Since the gaussian pulses may be viewed as a slowly-varying envelope at the electrical bit rate, numerical calculations of the sum of the $c_n''(t)$, with and without this approximation, have been computed by the authors

in order to establish the validity of this approximation. The expected variations in the order of 2% are fairly well reflected in the results. Under this assumption, and for a desired user, the signal after the decoder PM may be approximated by

$$s_{5,l}(t) \approx \sum_{n=-\infty}^{+\infty} |c_n|^2 \exp(\mathrm{j}\pi n^2 f_p \tau) s_{2,l}(t + n\tau, \Phi_1'' + \Delta\Phi'') \tag{19a}$$

$$S_{5,l}(f) \approx \sum_{n=-\infty}^{+\infty} |c_n|^2 \exp(\mathrm{j}\pi n^2 f_p \tau) \exp(\mathrm{j}2\pi n f \tau) S_{2,l}(f, \Phi_1'' + \Delta\Phi'') \tag{19b}$$

Finally, we will write the dispersion in the last LCFBG as $\Phi_4'' - \Phi_1'' - \Delta\Phi'' + \delta\Phi''$, for a total system net dispersion equal to $\delta\Phi''$. The output signal in the case of a desired user will then be approximated by

$$S_{6,l}(f, \Delta\Phi'', \delta\Phi'') \approx \sum_{n=-\infty}^{+\infty} |c_n|^2 \exp(\mathrm{j}\pi n^2 \tau f_p) \exp(\mathrm{j}2\pi n \tau f) \times s_{2,l}(f, \delta\Phi''), \tag{20a}$$

$$s_{6,l}(t, \Delta\Phi'', \delta\Phi'') \approx A_0'' \sum_{n=-\infty}^{+\infty} |c_n|^2 \exp(\mathrm{j}\pi n^2 \tau f_p) \times \exp\left(-\frac{1 + \mathrm{j}C''}{2}\left(\frac{t + n\tau}{\sigma T_0}\right)^2\right), \tag{20b}$$

where

$$C'' = C + \frac{(1 + C^2)\delta\Phi''}{2T_0^2}, \tag{21a}$$

$$\sigma = \sqrt{\left(1 + \frac{C\delta\Phi''}{2T_0^2}\right)^2 + \left(\frac{\delta\Phi''}{2T_0^2}\right)^2}, \tag{21b}$$

$$A_0'' = \frac{A_0}{\sqrt{\sigma}} \exp\left(j\frac{1}{2}\arctan\left(\frac{\delta\Phi''}{2T_0^2 + C\delta\Phi''}\right)\right) \tag{21c}$$

and the output signal depends on the net dispersion between modulators $\Delta\Phi''$ only through the parameter τ.

We will now discuss the form of the complex envelope for the received signal. Eq. (20b) describes a series of identical, linearly chirped, dispersion-broadened Gaussian pulses, separated at regular time intervals, each one affected by a different phase shift. The time separation between pulses τ and the phase shifts are entirely due to the dispersion mismatch between phase modulators, while the broadening and the chirp are related only to the total net dispersion mismatch.

When no net dispersion mismatch between modulators exists, $\tau = 0$, or

$$s_{6,1}(t, 0, \delta\Phi'') \approx A_0'' \exp\left(-\frac{1 + jC''}{2}\left(\frac{t}{\sigma T_0}\right)^2\right). \tag{22}$$

The decoded output for a desired user is then equal to the input Gaussian pulse, except for a pulse broadening represented by the expansion factorσ, a constant phase change (related to the phase of A_0'' and to the dropped constant terms in the phase change introduced by each LCFBG) and a change in the pulse chirp. If a net system dispersion of the appropriate sign (opposite to the sign of the prechirp C) and value is chosen, the decoded pulse may be even sharper than the input pulse. For a pulse broadening (and a corresponding peak power decrease) of a factor of 2, the net dispersion in the system for optimum output pulse compression would need to be around 113 ps/nm for an initial pulse with realistic FWHM time duration of 20 ps and prechirp factor of 3, corresponding to around 6.6 km of SMF. This suggests that the total net system dispersion $\delta\Phi''$ will not be a major limiting factor in the system performance.

When there is no net system dispersion, $\delta\Phi''$=0, and the decoded output for the desired user is written as

$$s_{6,1}(t, \Delta\Phi'', 0) \approx \sum_{n=-\infty}^{+\infty} |c_n|^2 \exp(j\pi n^2 \tau f_p) s_{1,l}(t + n\tau). \tag{23}$$

In other words, the output is the sum of several "copies" of the input pulse, each one of them affected by a different phase shift and time delay. Note however that the separation between pulses will generally be much smaller than the actual pulse width. The addition of these pulses will then appear as a single pulse, either very similar in shape and width to the original one when τ is small, or highly distorded by the destructive addition of components with different phases when τ is large. We may therefore expect deformed decoded pulses for large values of $\Delta\Phi''$, with several relative maxima and minima, making it extremely difficult to achieve good signal reception. In other words, according to this theoretical analysis, $\Delta\Phi''$ will probably be the major factor limiting the system performance.

Finding a closed-form expression for (23) is very difficult, due to the quadratic dependence of the phase factor that affects each pulse, together with the nontrivial dependence of the c_n Fourier coefficients on the chosen code. As a result, simulations are needed in order to evaluate the performance limits introduced by the net dispersion between modulators $\Delta\Phi''$, as well as on the join effect of the net dispersion between modulators and the total system net dispersion. As we will show through simulation, there is a trend towards higher performance degradation as $\Delta\Phi''$ increases, with quasi-periodic, seemingly erratic behaviour for relatively low values of this net dispersion. This results in the need of an accurate control of this value in order to guarantee optimum system performance.

3. FE-OCDMA encoder/decoder design and evaluation

In this section, we present the numerical simulation of a FE-OCDMA link based on the encoder/decoder pair shown in Fig. 2. The encoder/decoder will be analysed in two different setups: single-user and multi-user. In the single-user configuration, we will try to establish the main limiting factors in the proposed link. In particular, we will try to model numerically the effect of the parameters $\Delta\Phi''$ and $\delta\Phi''$ defined in the previous section, in order to validate our previous hypotheses about their role in the system performance degradation. In the multi-user configuration, we will evaluate the system performance in a realistic working environment, in terms of two main characteristics: Multi Access Interference (MAI) and Bit Error Rate (BER). For this purpose, we study the system when several users are sharing the network simultaneously in order to evaluate system performance degradation as the number of users increases. Although we choose a particular implementation for the simulated encoder/decoder, note that, since most of the physical phenomena involved are very similar to other possible alternative configurations, the results presented and conclusions drawn, could be considered to very probably apply to many other electrically configurable spectral phase encoding techniques.

We propose device characteristics for use at wavelengths close to 1550 nm. An LCFGB with a full-width half-maximum of 1.6 nm and a dispersion value of $|\Phi_i''| \approx 12\pi \times 1250$ ps/nm rad avoids ISI effects between pulses, since the effective group delay needed for a high speed system will be lower than 0.622 Gbit/s for the operation bandwidth. Note that the bandwidth of the LCFBG has been selected to take into account the spectrum spreading introduced by the phase modulator. It is also relevant to consider the device length L, because this parameter fixes total LCFBG dispersion, since $L = (\pi c/n_{\mathrm{eff}})\Phi_i''\Delta f$, where c is the speed of the light in vacuum and n_{eff} is the effective refractive index (typically 1.45 [25]). We obtain a realistic length $L \sim 15.5$ cm. The power loss of the LCFBG and optical circulator are taken as 0.3 dB.

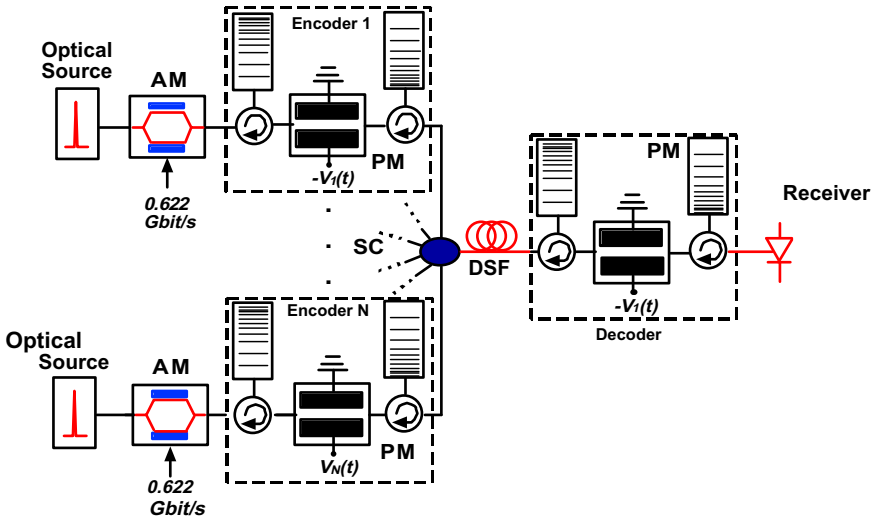

Fig. 1. OCDMA network setup for N simultaneous users an one receiver (AM: electro-optical amplitude modulator, LCFBG: linearly chirped Fiber Bragg Grating, PM: phase modulator and DSF: dispersion shifted fiber, SC: star couple).

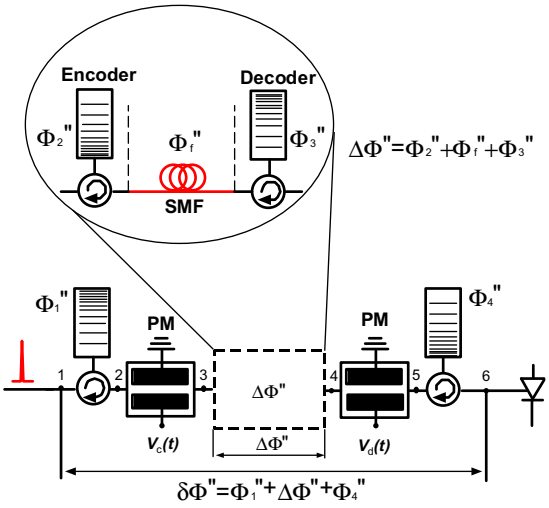

Fig. 2. Simplified model for the analysis of the overall system performance, showing the net dispersion between phase modulators $\Delta\Phi''$, and the global net dispersion $\delta\Phi''$. Numbers 1–6 show the positions in the system where signals $s_1(t)$ to $s_6(t)$ are present.

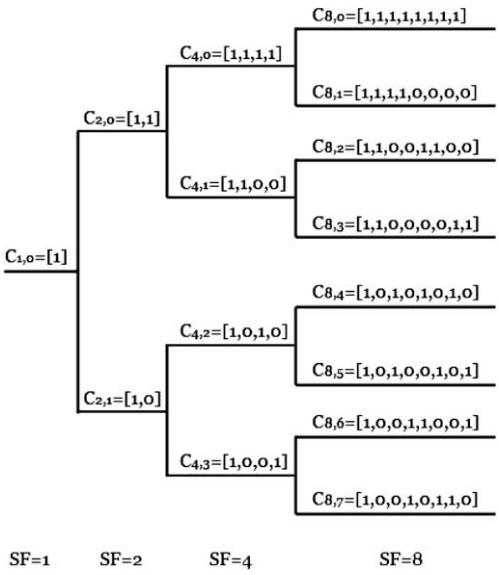

Fig. 3. Simplified tree structure of OVSF code with a depth 3, where $N = 8$.

Data and code bit rates BR_d and BR_c are related to the code length N through $N = BR_c/BR_d$. These are critical parameters, since we need to avoid high code bit rate (otherwise ISI would appear unless the system met very strict requirements) while not limiting the code length. For practical purposes, the data bit rate is fixed at 0.622 Gbit/s and the (realistic) maximum code bit rate is 20 Gbit/s when a 32 bit length code is used, or 10 Gbit/s for a 16 bit length code, respectively. We choose a source generating gaussian pulses with time width $T_0 \approx 24$ ps, or $T_{FWHM} \approx 50$ ps. While respecting the bandwidth restriction imposed at the LCFBG, this time duration is realistic for practical use. We choose a prechirp C equal to 5, because of the compromise between total generating dispersion and full bandwidth imposed by the LCFBG. We calculate a FWHM bandwidth for the chirped pulse of 33.81 GHz, and an approximate full bandwidth of 120 GHz at −30 dB. The most significant components of the power spectral density are well within the LCFBG bandwidth, resulting in a sharp pulse by ensuring the signal integrity.

In terms of the code, we chose 16- and 32-bit, 1D OVSF (Orthogonal Varible Spreading factor) orthogonal codes, used in mobile CDMA applications 3 G cellular communications [29]. OVSF codes are primarily used to preserve orthogonality between channels in a communication system [30,31], with different rates and spreading factors as can be expected in Passive Optical Network when different multimedia applications are multiplexing over one optical carrier. The OVSF codes are defined recursively by a tree structure, as shown in the Fig. 3.

If [C] is a code length 2^r at depth r in the tree, where the root has depth 0, the two branches leading out of C are labeled by the sequences [C, C] and [C, − C], which have length 2^{r+1}. The codes at depth r in the tree are the rows of the matrix C_N, where $N = 2^r$. This structure, allow OVSF codes a simple construction process at the same possibility extraordinary orthogonal properties which make attractive their use in optical applications. Note that two OVSF codes are orthogonal if and only if neither code lies on the path from the other code to the root. Since codes assigned to different users in the same link must be orthogonal, this restricts the number of available codes for a given network. The OVSF codes

Table 1
OVSF codes

Length	Desire user	Interference user
16	1010101010101010	1111000011110000
32	11001100001100111100110000110011	10011001100110011001100110011001

are converted to phase codes via the PM by assigning phase shifts of 0 and π to -1's and +1's, respectively. Such OVSF codes can provide a suitable autocorrelation and cross-correlation at the spectral width used in this work. Moreover we used a NRZ raised cosine shaped pulse with a roll-off factor of 0.8 for a more realistic description of the phase modulation. The codes used in the analysis are shown in Table 1.

Finally, the receiver consists on an optical thresholder, where a decoded pulse is detected if the received optical power value exceeds an adequately chosen value at an appropriate time instant, and no pulse is decoded otherwise. This type of detection schemes has been used, for example, in [32,33].

For the simulation of BER and MAI, the optical link used in transmission includes 20 km of dispersion-shifted fiber (DSF) with 0.2 dB/km loss [34]. DSF exhibits a zero-dispersion value around the 1550 nm wavelength and minimum attenuation. It is possible to employ other types of single-mode fibers, such as S-SMF or NZD (NonZero-Dispersion fiber), but as evidenced by the single-user simulations, this could require the use of a dispersion compensating module in order to avoid catastrophic system performance degradation. Such a compensating system could be included in the LCFBG design for known link lengths. For *a priori* unkown link lengths, tunable dispersion compensation is also available [24].

Simulations were carried out using Optsim 4.1 by Rsoft Inc. Other simulation parameters are given in Table 2.

3.1. Single-user configuration

A single user configuration was simulated in order to establish the effect of the main limiting factors in the system performance, namely the net dispersion between modulators $\Delta\Phi''$ and the net total system dispersion $\delta\Phi''$, defined in Fig. 2.

The effect of the net dispersion between modulators $\Delta\Phi''$ was first modelled, the results being shown in Figs. 4 and 5. The total net dispersion $\delta\Phi''$ was kept equal to zero by introducing an appropriate dispersive element between encoder and decoder, and adding a compensating dispersion of opposite sign after the decoding modulator. Fig. 4 shows the evolution of the maximum peak power and time width of the decoded pulse. These two parameters, which may be used to described quantitatively the decoded pulse quality, seem to have a quasi-periodic behaviour for small values of the net dispersion between modulators, the former rising when the latter decreases, indicating a sharper pulse. For sufficiently high values of the net dispersion between modulators, a tendency towards higher pulse degradation with increasing dispersion may be observed.

Table 2
Simulation parameters

Symbol	Parameter	Value
$\mathscr{R}$	Responsivity	0.7 A/W
RIN	Source RIN noise	-150 dB/Hz
$\Delta\Phi'' pt$	Photodetector Bandwidth	40 GHz
Δf	LCFBG bandwidth	1.6 nm
Φ''	LCFBG dispersion slope	$(1/2\pi)$1250 ps/nm?rad
V_0	Zero phase voltage	0 V
V_π	Phase voltage π	5 V
BW_{ph}	Phase modulator $-$ 3 dB bandwidth	40 GHz
λ_o	Central wavelength	1550 nm
BW_{mod}	Mach–Zhender $-$ 3 dB bandwidth	10 GHz
C	Source chirp factor	5
BR_c	Code bit rate	10, 20 Gbit/s
BR_d	Data bit rate	0.622 Gbit/s
k	Modulator excess loss	3 dB
T_0	Pulse half width	24 ps
T_{FWHM}	Full-Width Half-Maximum	50 ps
B_o	Gaussian pulse bandwidth	120 GHz
N	Code length	16, 32
P_{opt}	Source average power sweep	1–15 mW

For the results of Fig. 4 to be complete, we need to assess not only the width and peak power of the decoded pulse, but also its shape. For selected values of the net dispersion between modulators, indicated in Fig. 4, the resulting decoded pulses are shown in Fig. 5. It may be observed that, for a net dispersion of 18 ps/nm, the decoded pulse is nearly equal to the decoded pulse in the (ideal) zero net dispersion case. Up to a net dispersion of close to twice this value, the decoded pulse may be considered "identical" to the ideal case for all practical purposes; the individual pulses added in the left-hand side of Eq. (19a) are very close together in time, and affected by phase factors very close to unity, since τ is very small. We may therefore establish an upper bound for the dispersion tolerance of approximately 30–35 ps/nm, or equivalently 2 km of SMF, consistent with PON access network lengths. For higher values, the system performance quickly degrades, and for a net dispersion of 44 ps/nm, the information may be considered to be completely lost. For higher values of the net dispersion, such as 144 ps/nm, although the pulse peak power and time width are again comparable to, or even better than, the zero dispersion case, the pulse shape is not completely regular, exhibiting a maximum not at $t = 0$, and local maxima and minima. This behaviour may result in errors unless the decision threshold and decision time are very precisely controlled. In these last two cases, the separation between the individual pulses added in Eq. (19a) has significantly grown, as has the phase difference between them, thus effectively broadening the total received signal, and producing maxima and minima as a consequence of the alternating constructive and destructive interference. Note finally that the complex behaviour shown in Figs. 4 and 5 with respect to the net dispersion in the modulator is due to the highly nonlinear dependence on the pulse shape as predicted in Eq. (20b).

Finally, the effect of the total system net dispersion was modelled, for selected values of the net dispersion between modulators. This was achieved by introducing a dispersive element between encoder and decoder, fixing $\Delta\Phi''$, and then adding a variable dispersion after the decoding modulator, producing in each case the desired value of $\delta\Phi''$. The results of this simulation are shown in Fig. 6. When the net dispersion between modulators is 0 or 18 ps/nm (zero net dispersion or nearly identical received pulse shape) the pulse width and peak power change smoothly and monotonically with the net system dispersion, producing pulse compression or dilation. Note that the trend towards compression or dilation is opposite in both cases, the net dispersion between modulators having inverted the original ordering of the frequency components inside the pulse. For values of the net dispersion between modulators producing a large pulse degradation, such as 44 ps/nm, the dependence of the decoded pulse shape on the net dispersion is very small, the net dispersion between modulators

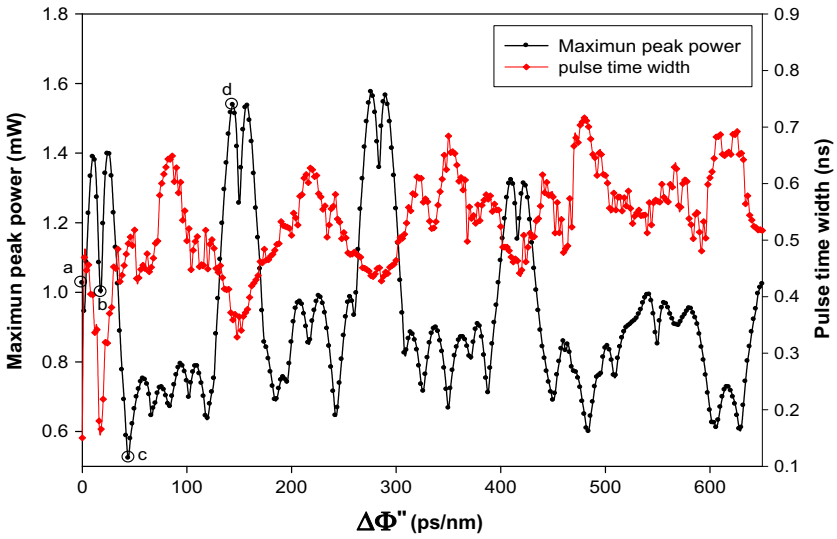

Fig. 4. Simulated decoded pulse time width and maximum peak pulse power for different values of the net dispersion between modulators $\Delta\Phi''$. The total net dispersion in the link $\delta\Phi''$ was kept equal to zero by introducing a compensating dispersion after the decoder modulator. Highlighted points correspond to values of the net dispersion between modulators of 0, 18, 44 and 144 ps/nm.

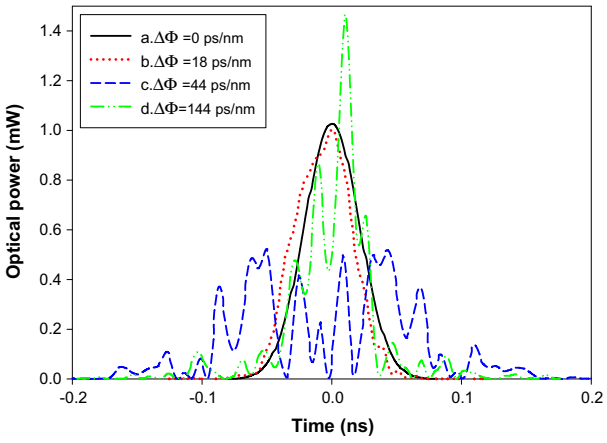

Fig. 5. Decoded pulse shapes for selected values of the net dispersion between modulators: 0, 18, 44 and 144 ps/nm. The corresponding simulated pulse widths and peak powers are highlighted in Fig. 4.

being the main factor, and fully responsible for the pulse degradation. Finally, for values of the net dispersion between modulators producing irregularly shaped pulses with high peak powers and low time widths, such as 144 ps/nm, the behaviour of the pulse peak power is erratic, while the pulse width is nearly constant. This is because a small broadening or compression in the time-shifted, phase-shifted gaussian pulses that add in the output signal has a small effect in the overall pulse duration, but at the same time the width change may significantly alter the amount that each of the individual components brings to the constructive or destructive addition that produces the output signal.

It is important to stress that, although the theoretical analysis shown in Section 2 contains an approximation, the intuitive conclusions from this theoretical study match very well, and satisfactorily explain, the simulated results, supporting the validity of the approximation performed and the conclusions derived.

3.2. Multi-user configuration

We finally present the simulation results for the configuration shown in Fig. 1 in the presence of multiple user access, for the ideal case of no dispersion mismatch, i.e., zero net dispersion between phase modulators $\Delta\Phi'' = 0$, and zero global net dispersion $\delta\Phi'' = 0$. The simulation parameters are those shown in Tables 1 and 2. In order to quantify the link performance, we have simulated the pulse shape decoded by a non-desired user, as well as the Bit Error Rate introduced on the desired user by Multiuser Interference.

Fig. 7 shows the autocorrelation and cross-correlation responses to OVSF codes with 16 and 32 bit elements, respectively, when the OCDMA network is operating with 1 user in back to back configuration, at 0.622 Gbps. The solid line (~90 ps long pulse with high peak power) corresponds to the autocorrelation trace, while the dotted line corresponds to the cross-correlation trace and presents a maximum time width of 1.6 ns.

The autocorrelation is very similar for both length codes, although a zoomed view shows a slightly better result in the 32-element case. The longer code provides however a visibly better cross-correlation profile. Intuitively, when an incorrect code is applied to the decoder, a time redistribution of the optical power significantly broadens and depresses the output power, due to the fact that the weight functions $c_n''(t)$ do not present anymore a constant sum, but time-varying terms that will suffer very different time delays at the last LCFBG, are present at the PM output.

The more constant distribution of the optical power in the cross-correlation for the 32-element code is due to the fact that more terms are relevant in the Fourier series describing the PM drive signal, thus more terms with highly non-linear (quasi-random) phases contribute to the generation of the output pulse. However, the absence of significant (compared to the autocorrelation pulse peak power) lobes in the cross-correlation profile for both the 16- and 32-element OVSF codes cross-correlation profiles demonstrates the practical feasibility of the system. The results shown are comparable to those published for other OCDMA spectrally encoded systems [20,23,35–37].

We will now characterize the quality of the system under multi-user operation. In order to evaluate the system performance, we let the optical source power vary from 1 to 15 mW, using otherwise the same parameters as in Section 3.1. The effect of up to six users (one "desired" and six "interfering") was simulated. The Bit-Error-Rate (BER) diagrams for N users simultaneously transmitting at 622 Mbps using 16- and 32-element codes are shown in Fig. 8. The BER of the test-bed is taken with respect to the received power

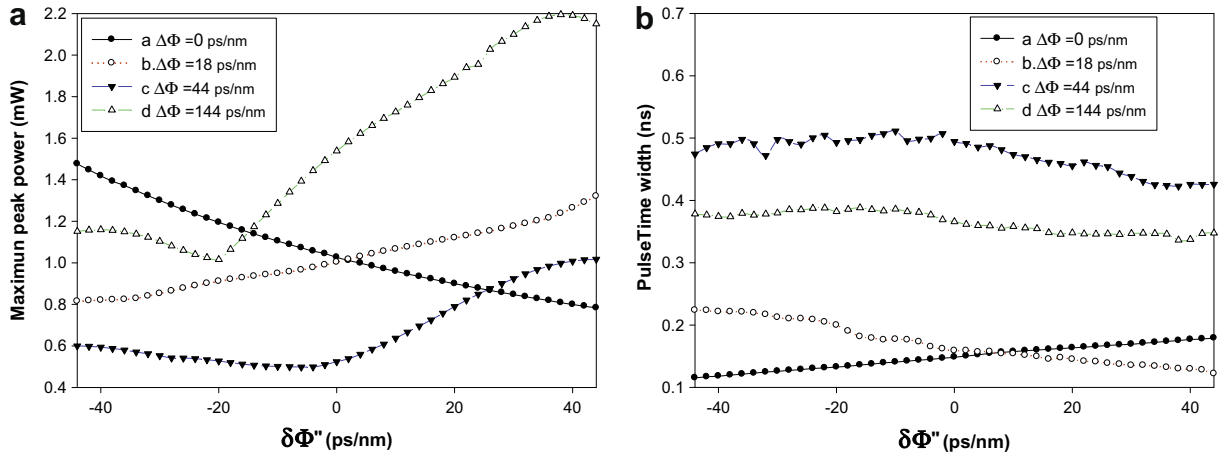

Fig. 6. Simulated decoded pulse maximum power (a) and pulse time width (b) as a function of the total net dispersion in the link, for selected values of the net dispersion between modulators (0, 18, 44 and 144 ps/nm). The corresponding values for zero total net dispersion are highlighted in Fig. 4.

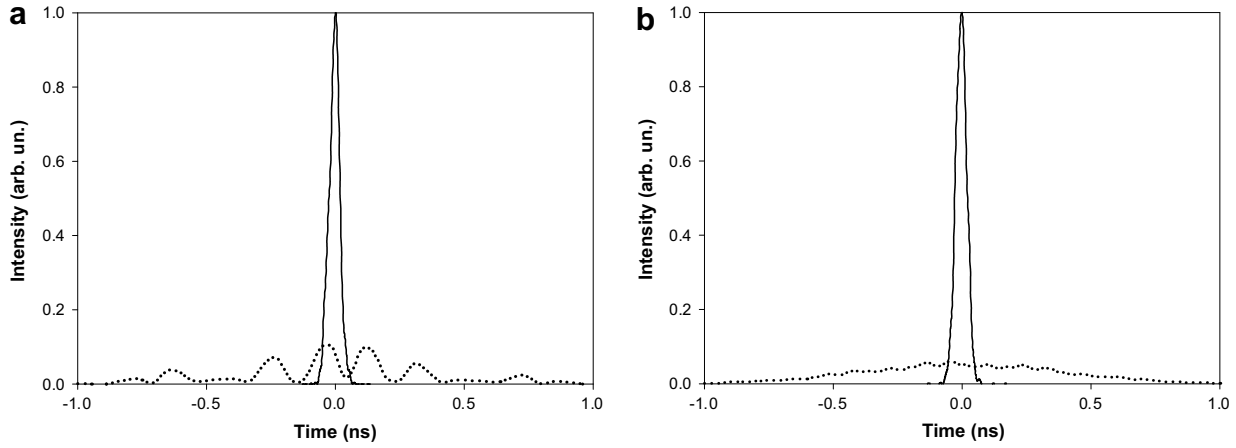

Fig. 7. Optical signal after decoding, using the correct OVSF code (thick solid line) and an incorrect code (dotted line), (a) for a 16-element code and (b) for a 32-element code.

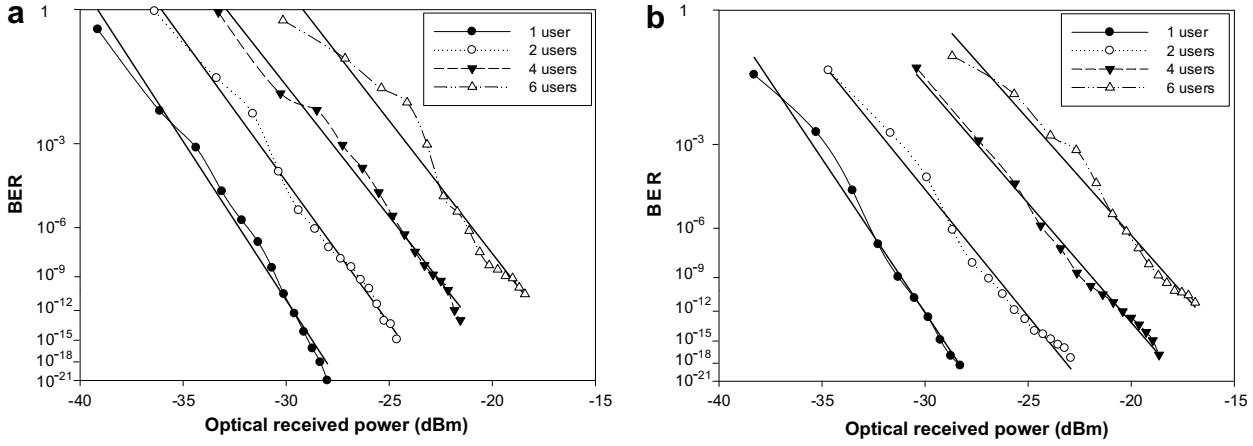

Fig. 8. BER curves at 622 Mbps bit rate, using (a) 16- and (b) 32-element OVSF code, and from 1 to 6 users transmitting simultaneously, sharing the optical network.

at the end of the decoder just before the photo-detector. As shown in Fig. 8a, a minimum optical power of −30 dBm is required to ensure a BER of 10^{-9} when only one uses utilizes the network. A power penalty of ~4 dB is observed as each additional user is included. This penalty is primarily due to two effects: the increase in shot noise, and residual cross-correlation from signals destined to the "interfering" users (MAI). The BER change from 10^{-6} to 10^{-8} occurs over a longer power range in the case of multi-user ac-

cess, as expected from this interference; in other words, for a given BER performance, each additional user introduces a higher power penalty, because of the simultaneous action of the two effects mentioned above.

BER curves with 32-element OVSF codes (Fig. 8b) have lower power penalties in comparison with 16-element codes. In single user configuration the sensitivity is improved by ~2 dB due to the better correlation relations that the long codes present (as discussed before). The power penalties are also lower, relative to 16-element codes, with two or more users due to a reduction of the interference.

In accordance with the theoretical study and the results obtained through simulation, it may be possible to increase the system bit rate to improve transmission features. This will result in a reduction in the dispersion needed from each LCFBG, since a higher bit rate will result in a shorter pulse duration and required delay. However, higher electrical code rate at the encoder/decoder will be necessary, resulting in increased BER and reduced power sensitivity at 2.5 Gbit/s due to frequency limitations in the system under study.

Finally, note that although the effect of coherent beat noise may be important in the system performance, it has been shown that an adequate choice of the threshold level in the receiver may significantly improve the BER in OCDMA schemes [38]. The BER curves shown in Fig. 8 are actually calculated by assuming an optimum sampling time and thresholding value, leading to MAI being the main source of errors in the receiver.

4. Conclusions

We have provided a theoretical analysis and evaluation through simulation of an electrically configurable encoder/decoder, with applications in OCDMA, which relies on dispersion and phase modulation in order to achieve spectral phase encoding. The encoder/decoder is simple, flexible, and scalable because the optical hardware (readily available commercial devices) is independent on the code family used. The theory and simulation results presented apply not only to our chosen configuration, but also to other particular implementations, one of them has been recently demonstrated experimentally.

The theoretical model developed and presented, as well as the numerical simulations performed, point at the net dispersion mismatch between modulators as the main cause for system degradation. Although the system performance quickly degrades as this parameter increases, the technique is applicable in LAN and PON environments, since the dispersion introduced by the usual lengths of SMF in these scenarios is still tolerable by the system. Furthermore, careful design of the last dispersive elements, together with tunable dispersion compensation, may be used to ensure robust system performance, even over longer distances; the same effect may be achieved by transmitting the signal over DSF. The other critical parameter in the system performance, which is the total net dispersion in the entire system, is shown to have little effect for SMF lengths consistent with LAN or PON environments. The results also suggest very strongly that a certain mismatch in the LCFBGs is also perfectly tolerable, as long as this mismatch does not result in values of the net dispersion between modulators or net total system dispersion high enough to produce performance degradation.

Although approximations are used in the derivation of the theoretical model, numerical simulations strongly suggest that the approximated close-form results are in fair agreement with reality, especially since the intuitive explanation of the simulated results agrees with the conclusions drawn from the theoretical study.

Simulated BER performance under multi-user operation (up to six simultaneous users over a 20 km DSF fiber optical transmission link) is also presented. These simulations are very useful in determining expected values for the minimum power required for error-free operation, as well as for the power penalty introduced by each simultaneous additional interfering user sharing the network.

Acknowledgments

The authors wish to acknowledge C. Rodés, D. Gómez, S. Tainta, M.J. Erro, M.J. Garde, M.A. Gómez-Laso and J. Sevilla for valuable discussions.

References

[1] P.R. Prucnal, M.A. Santoro, T.R. Fan, J. Lightwave Technol. 4 (1986) 547.
[2] J.A. Salihi, C.A. Brackett, IEEE Trans. Commun. 37 (1989) 824.
[3] M.E. Marhic, J. Lightwave Technol. 11 (1993) 854.
[4] P.C. Teh, P. Petropoulos, M. Ibsen, D.J. Richardson, IEE Electron. Lett. 3 (2001) 190.
[5] P.C. Teh, P. Petropoulos, M. Ibsen, D.J. Richardson, IEEE J. Lightwave Technol. 9 (2000) 1352.
[6] X. Wang, K. Matsushima, A. Nishiki, N. Wada, K. Kitayama, Opt. Express 12 (2004) 5457.
[7] N. Wada, K. Kitayama, IEEE J. Lightwave Technol. 17 (1999) 1758.
[8] T.J. Eom, S.-J. Kim, T.-Y. Kim, C.-S. Park, U.-C. Paek, B.H. Lee, IEEE J. Lightwave Technol. 23 (2005) 597.
[9] S. Yegnanarayanan, A.S. Bhushan, B. Jalali, IEEE Photon. Tech. Lett. 12 (2000) 573.
[10] L.R. Chen, P.W.E. Smith, IEEE Photon. Tech. Lett. 12 (2000) 1281.
[11] V. Baby, I. Glesk, R.J. Runser, R. Fischer, Y.K. Huang, C.S. Bres, W.C. Kwong, T.H. Curtis, P.R. Prucnal, IEEE Photon. Technol. Lett. 17 (2005) 253.
[12] Y.K. Huang, V. Baby, P.R. Prucnal, C.M. Greiner, D. Iazikov, T.W. Mossberg, IEEE Photon. Tech. Lett. 17 (2005) 825.
[13] U.N. Griner, S. Arnon, IEEE Photon. Tech. Lett. 16 (2004) 332.
[14] H. Fathallah, L.A. Rusch, S. LaRochelle, IEEE J. Lightwave Technol. 17 (1999) 397.
[15] S. Ayotte, M. Rochette, J. Magne, L.A. Rusch, S. LaRochelle, IEEE J. Lightwave Technol. 23 (2005) 724.
[16] S. Etemad, P. Toliver, R. Menendez, J. Young, T. Banwell, S. Galli, J. Jackel, Delfyett, C. Price, T. Turpin, IEEE Photon. Tech. Lett. 17 (2005) 929.
[17] H. Tsuda, H. Takenouchi, T. Ishii, K. Okamoto, T. Goh, K. Sato, A. Hirano, T. Kurokawa, C. Amano, IEE. Electron. Lett. 35 (1999) 1186.
[18] Z. Zheng, A.M. Weiner, K.R. Parameswaran, M.H. Chou, M.M. Fejer, IEEE Photon. Technol. Lett. 13 (2001) 376.
[19] J. Huang, D. Hsu, IEEE Photon. Tech. Lett. 12 (2000) 1252.
[20] P.A. Lacourt, S.E. Ralph, S. McLaughlin (Eds.), Proceedings of the Conference on Lasers and Electro-Optics, 2004.
[21] A. Agareal, P. Toliver, R. Menendez, T. Banwell, J. Jackel, S. Etemad, IEEE Photon. Tech. Lett. 18 (2006) 1952.
[22] A. Andueza, D. Benito, URSI XII (2006) 1042.
[23] X. Wang, N. Wada, Opt. Express 15 (2007) 7319.
[24] M.J. Erro, M.A.G. Laso, D. Benito, M.J. Garde, M.A. Muriel, IEEE J. Select. Top. Quantum Electron. 5 (1999) 1332.
[25] J. Azaña, M.A. Muriel, IEEE J. Quantum Electron. 36 (2000) 517.
[26] N. Henmi, T. Saito, T. Ishida, J. Lightwave Technol. 12 (1994) 1706.
[27] T.L. Koch, R.C. Alferness, J. Ligthwave Technol. 3 (1985) 800.
[28] J.E. Roman, K.A. Winick, IEEE J. Quantum Electron. 29 (1993) 975.
[29] 3GPP TS 25.213, Third Generation Partnership Project; Technical Specification Group Radio Access Network; Spreading and modulation (FDD), (Release 6) 3GPP, 2005.
[30] R.G. Cheng, "A code management mechanism for WCDMA mobile communication networks," In: International Workshop on Mobile Communications, Crete, June 1999, p. 348.
[31] Y.-C. Tseng, C.-M. Chao, IEEE Trans. Mobile Comput. 1 (4) (2002) 293.
[32] X. Wang, T. Hamanaka, N. Wada, K. Kitayama, Opt. Express 13 (2005) 5499.
[33] K. Kravtsov1, P.R. Prucnal1, M.M. Bubnov, Opt. Express 15 (2007) 13114.
[34] K.S. Kim, R.H. Stolen, W.A. Reed, K.W. Quoi, Opt. Lett. 19 (1994) 257.
[35] H.P. Sardesai, C.-C. Chang, A.M. Weiner, J. Ligthwave Technol. 16 (1998) 1953.
[36] H. Sotobayashi, W. Chujo, K. Kitayama, IEEE J. Select. Top. Quantum Electron. 10 (2004) 250.
[37] V.J. Hernandez, Y. Du, W. Cong, R.P. Scott, K. Li, J.P. Heritage, Z. Ding, B.H. Kolner, S.J. Ben Yoo, IEEE J. Lightwave Technol. 22 (2004) 2671.
[38] X. Wang, K. Kitayama, J. Lightwave Technol. 22 (2004) 2226.